PCCP

Accepted Manuscript

ROYAL SOCIETY OF CHEMISTRY

www.rsc.org/pccp

Cite this: DOI: 10.1039/c0xx00000x

www.rsc.org/pccp

PERSPECTIVE

Recent advances in synthesis and applications of clay-based photocatalysts: a review

Jin Liu[a] and Gaoke Zhang*[ab]

Received (in XXX, XXX) Xth XXXXXXXXX 20XX, Accepted Xth XXXXXXXXX 20XX

DOI: 10.1039/b000000x

Clay materials including clay minerals and layered double hydroxides (LDHs) have attracted great attention for their special layer structures, large specific surface areas, remarkable adsorption capacities. In the past decades, they have been regarded as important components or precursors for making various functional materials. This paper aims to review and summarize the recent advances on the synthesis and photocatalytic applications of clay-based photocatalysts. Moreover, the effects of surface and structure characteristics of clay-based photocatalysts on photocatalytic properties are also discussed. The clay-based photocatalysts show good application prospect for environmental remediation and energy conversion. Especially, H_2 generation and reduction of CO_2 into carbon sources can be easily achieved by the LDH-based photocatalysts. Meanwhile, the role of clay materials in the photocatalysis is discussed in detail.

1 Introduction

Recent decades, environmental pollution and energy shortages have raised awareness of a potential global crisis. For the sustainable development of human society, the development of non-pollution and low-energy consumption technologies for environmental remediation is an urgent task. A great number of researches are being carried out in the development of advanced oxidation processes (AOPs) for the treatment of wastewaters, which usually operate at mild temperature and pressure. Among the AOPs, photocatalysis employing semiconductor catalysts such as TiO_2,[1-6] ZnO,[7-9] Bi_2WO_6,[10-13] CdS,[14-17] Bi_3NbO_7,[18-21] Zn_2GeO_4,[22-25] Ag/AgCl[26, 27] has demonstrated its efficiency in degrading refractory organics into readily biodegradable compounds, and eventually mineralized them to innocuous CO_2 and H_2O. Photocatalytic H_2 generation or reduction of CO_2 into carbon sources such as CO, HCOOH, HCHO, CH_3OH and CH_4 is a potential method for solving both energy and environmental problems, which shows good application prospect and thus has been widely reported.[28-35] From the point of view of semiconductor photochemistry, photoexcitation of electrons (e^-) and holes (h^+) are generated when the energy of the incident photons matches or exceeds the bandgap of semiconductor. Some e^- and h^+ will interact with electron acceptors or donors adsorbed on the surface of photocatalysts. However, the e^- and h^+ can be trapped in surface or deep traps or they can recombine non-radiatively or radiatively, resulting in producing heat or photoemission, respectively, which results in low efficiency of photocatalysis.[36-38] In the past decade, morphological design, non-metal or metal doping and coupling semiconductors with other materials have been employed to improve the photocatalytic performance of photocatalysts.[39-51] However, the photocatalytic efficiency of photocatalyst with small specific surface area and low adsorption capacity is relatively low in very dilute solution. In addition, most of nanometer-scale photocatalysts are not easily separated in suspension after use, which hinders their large-scale industrial application. Hence, the development of photocatalysts with high adsorption capacity and good sedimentation properties is important.

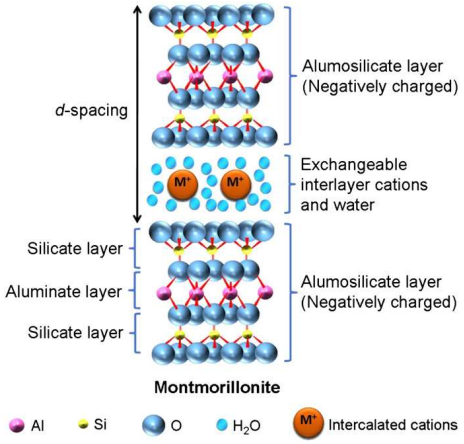

Fig. 1 Schematic illustration of the layer structure present in montmorillonite clay. Adapted from ref. 55 with permission. Copyright 2012, Elsevier.

Clay materials could be categorized into clay minerals (cationic clays) and layered double hydroxides (anionic clays). Clay minerals are typically composed of aluminosilicate layers, which consist of one (for 1:1-type) or two (for 2:1-type) Si–O tetrahedral sheets and one Al–O (Mg–O) octahedral sheet. The layers in the 2:1-type clay minerals (e.g., montmorillonite, sepiolite and attapulgite) are bound together by both electrostatic and hydrogen bonding forces. Moreover, they have an excess of

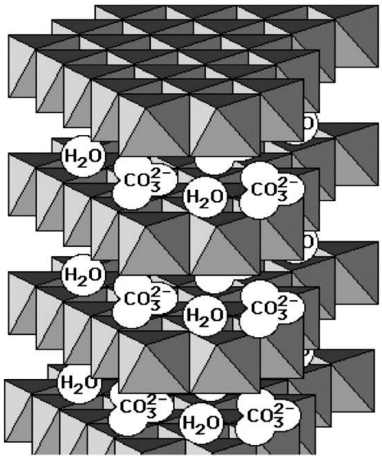

Fig. 2 The structure of a layered double hydroxide, with interlayer carbonate anions. Adapted from ref. 60 with permission. Copyright 1999, Elsevier.

negative surface charge due to the presence of non-equivalent, isomorphic substitutions of the central atoms within the tetrahedral (e.g. Al for Si) and/or octahedral sheets (e.g. Mg for Al). Accordingly, the negative charge can interact strongly by electrostatic forces with charge balancing cations, typically alkali metal ions, existed in the interlayer space (Fig. 1). Consequently, 2:1-type clay minerals possess unique physicochemical properties such as large surface area, high adsorption capacity, swelling and ion exchange, which can be adjusted by exchanging the cations in the interlayer space or treating with acids. [52-55] Up to now, they have been widely used in adsorption and catalytic fields.[56-59] In particular, clay minerals are non-corrosive, low-cost, and can be separated easily in reaction system for reuse.

LDHs are natural or synthetic mixed metal hydroxides, which can be easily obtained by a large scale and low cost approach. LDHs are described as the general formula $[M_{(1-x)}^{2+}M_x^{3+}(OH)_2]^{x+}A_{x/n}^{n-}\cdot mH_2O$, where M^{2+} and M^{3+} are the divalent (e.g., Mg^{2+}, Co^{2+}, Ni^{2+}, Zn^{2+}, Cu^{2+})and trivalent cations (e.g., Al^{3+}, Fe^{3+}, Ga^{3+}) and A^{n-} are the anions (e.g., CO_3^{2-}, SO_4^{2-}, NO_3^-). The structure of LDHs is similar to that of brucite ($Mg(OH)_2$) as shown in Fig. 2, where hydroxyl anions are hexagonally close packed and magnesium cations are filling all octahedral sites every two layers. Consequently, the edge-sharing octahedra of cations are surrounded by six hydroxyl groups (–OH) forming brucite-like sheets. These sheets are stacked on top of each other and are held together by hydrogen bonding. When the M^{2+} cations are replaced by M^{3+} cations, positive charges can form in the brucite-like sheets. The charge density and the anion exchange capacity of the LDHs may be controlled by varying the M^{2+}/M^{3+} ratio. A^{n-} are located within the interlayer gallery together with the water molecules for balancing the positive charges.[60, 61] Recently, synthetic LDHs have also received growing interest in fields such as adsorption, catalysis, electrochemistry, and biotechnology due to their large specific surface area, high anion-exchange capacity, layered structure and good thermal stability.[61-66]

The above clay materials have specific features like their nanometer-scale layers and interlayers and their capacity for versatile tuning of the components on layers and within interlayers, so they are very suitable to be designed and transformed into function materials.[67-69] Recent years, clay materials are widely used as supports and their special layer structures, large specific surface area, high adsorption capacity are good for the enrichment of organic pollutants and the load of semiconductor. Based on our prior researches, in some cases, the introduction of clay materials into the clay-based photocatalysts can change the phases of semiconductor or improve the separation of e^- and h^+. So far, the clay-based photocatalysts such as TiO_2/montmorillonite,[70] TiO_2/sepiolite,[71] TiO_2/kaolinite,[72] ZnO/bentonite,[73] TiO_2/Zn-Al LDH,[74] TiO_2/Mg-Al LDHs,[75] SnO_2/Mg-Al LDH[76] have been reported. Clay-based photocatalysts are not only applied for photocatalytic degradation pollutants, but also are used for photocatalytic H_2 generation or reduction of CO_2. Moreover, compared to the pure semiconductor photocatalysts, these composite photocatalysts show enhanced photocatalytic properties and can be easily recovered from the solution.

The overall objective of this review is to present case studies of clay-based photocatalysts, including the natural clay mineral-based photocatalysts and synthetic LDH-based photocatalysts. The synthesis, modification and photocatalytic applications of the clay-based photocatalyts have been discussed in detail. A fresh insight into understanding the role of the clay materials for the photocatalysis has also been gained.

2 Synthesis and photocatalytic applications of clay mineral-based photocatalysts

2.1 Synthesis of clay mineral-based photocatalysts

A variety of semiconductors have been used for the synthesis of clay mineral-based photocatalysts. They mainly include metal oxides (e.g., ZnO,[73] TiO_2[77, 78]), salts (e.g., ZnS,[79] CdS[80, 81]) and silver/silver halides (Ag/AgCl[82], Ag/AgBr[83]). The commonly used preparation methods are sol-gel method, hydrothermal method and solution mixing method. The following subsections will give a more detailed introduction of the available synthesis methods.

2.1.1 Sol-gel method

Sol-gel method has been widely used for the synthesis of metal oxides which mainly includes hydrolysis polymerization, drying and thermal treatment stages. It also can be adopted for the pillaring of the clay minerals with the semiconductors. The pillaring procedures for the preparation of pillared clay (PILC) composites are usually considered to be: (i) swelling of clays in water; (ii) exchanging the cations in the interlayer of clay by partially hydrated polymeric or oligomeric metal cation complexes; (iii) drying and calcining of the wet cake of expanded clay to transform the metal polyoxocations into metal oxide pillars.[84] After pillaring, stable porous structures and lots of active sites in the pillared clay composites were presented. The intercalation of TiO_2 into the interlayer of clays is one of the most promising methods for synthesizing TiO_2 pillared clay composites with enhanced photocatalytic activity. For example, Ding *et al.*[85] prepared TiO_2 PILC composite by a traditional sol-gel method. Different drying methods such as air drying, air drying after ethanol extraction, and supercritical drying have been employed, resulting in different crystallite sizes of TiO_2. Zhang *et al.*[77] synthesized TiO_2 pillared montmorillonite composite with the anatase phase of TiO_2 without calcination via hydrolyzing

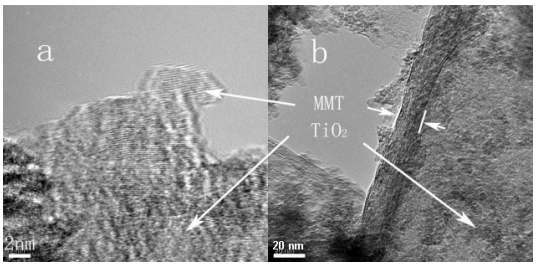

Fig. 3 TEM of TiO_2 pillared montmorillonite. Adapted from ref. 77 with permission. Copyright 2008, American Chemical Society.

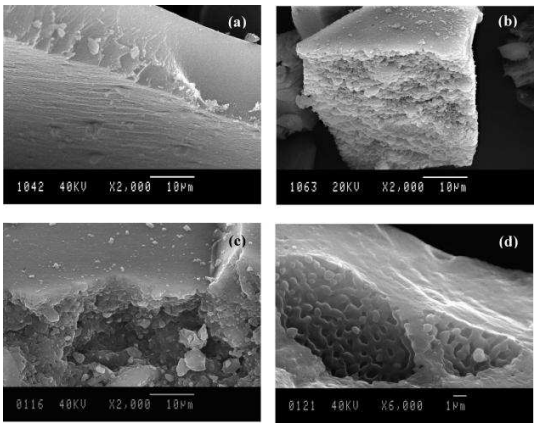

Fig. 4 SEM images of (a) PILC550, (b) PILC1000, (c,d) PILC1200. Adapted from ref. 86 with permission. Copyright 2008, American Chemical Society.

$TiCl_4$ into HCl aqueous solution and then impregnating Ti-polycations into the interlayer of montmorillonite through the ion-exchange. From Fig. 3, it can be seen that the intercalation of TiO_2 nanoparticles into the interlayers of montmorillonite destroyed the ordered structure of montmorillonite to some extent, resulting in some exfoliated one-layer and multilayer sheets. TiO_2 nanoparticles were formed in the interlayers of montmorillonite and on the surface of montmorillonite during the hydrolysis process of the precursor. Lim *et al.*[86] synthesized TiO_2 pillared laponite composite by adding the clay suspension to the Ti^{4+}-containing mix and stirring for 3 h before a hydrothermal treatment and then calcining the precursor at different temperature. The structures of samples calcined at 550 °C (PILC550), 1100 °C (PILC1100), 1200 °C (PILC1200) are shown in Fig 4. Compared to Fig. 4a, it is noted that the heat treatment at higher temperatures (1000 or 1200 °C) has caused disorder in the layered structures of PILC1000 and PILC1200. Chen *et al.*[87] prepared a series of SiO_2 and TiO_2 co-pillared montmorillonite composites with excellent adsorption capacity and high photocatalytic activity by pillaring both SiO_2 and TiO_2 mixed sol into Na-montmorillonite. The results showed that high content of SiO_2 in the pillared montmorillonite was in favor of large adsorption capacity, while high content of TiO_2 in the co-pillared montmorillonite was beneficial for the high photocatalytic activity. Recently, Chen *et al.*[88] reported TiO_2 pillared clay composite which was prepared by montmorillonite and acidic solutions of hydrolyzed Ti alkoxides using a polymeric surfactant POP-D2000 as expanding agent (Fig. 5). Introducing polymer surfactant as an expanding agent of montmorillonite not only promote the formation of the delaminated structure, but also significantly improve the porosity and specific surface area of the

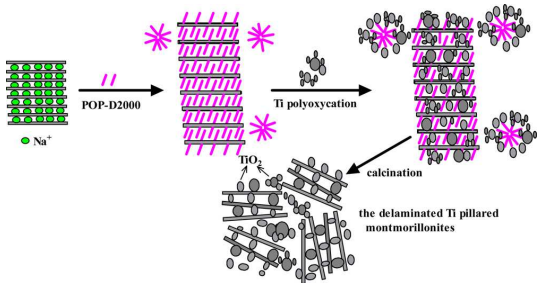

Fig. 5 Schematic illustration for preparation of the porous Ti pillared montmorillonites with a delaminated structure. Adapted from ref. 88 with permission. Copyright 2012, Elsevier.

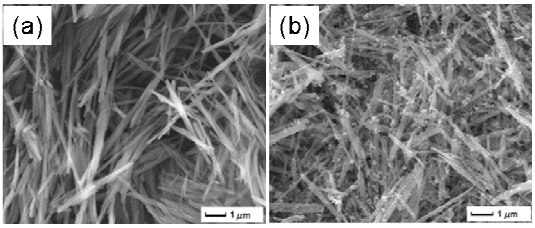

Fig. 6 SEM images of (a) HNTs and (b) CdS/HNTs. Adapted from ref. 81 with permission. Copyright 2012, Elsevier.

TiO_2 pillared clay composite. In order to use the TiO_2 pillared clay mineral composite for the degradation of pollutants under the visible-light irradiation, metal or nonmetal-doped TiO_2 pillared clay mineral composites were explored. For example, N,S-TiO_2 pillared montmorillonite composite was successfully synthesized via impregnating doped titania sol into the interlayers of montmorillonite, using $TiCl_4$ and thiourea ($CS(NH_2)_2$) as a precursor of TiO_2, N and S, respectively.[89] Besides, other non-TiO_2 pillared clay mineral composites have been synthesized. For example, Guo *et al.*[90] intercalated the amorphous citrate gel contained Bi and W elements into the interlayer of rectorite. After calcination treatment, the Bi_2WO_6 particles were formed in the interlayers of rectorite and on the surface of rectorite.

2.1.2 Other methods

Apart from sol-gel method, other methods such as hydrothermal method, solution mixing method are also used for the synthesis of clay mineral-based photocatalysts. For example, Xiao *et al.*[80] prepared the CdS/rectorite nanocomposite by hydrothermal method. The hydrothermal processes led to the formation of CdS nanoparticles with larger particle size and more perfect crystal as well as obvious changes in microstructures of the rectorite. The CdS nanoparticles existed in the rectorite layers and their size was smaller than that of CdS in the physical mixture of CdS and rectorite. In addition, the band gap energy of CdS intercalated composites was larger than that of the physical mixture of CdS and rectorite. The similar result was also reported by Fatimah *et al.*[91] Xing *et al.*[81] synthesized CdS/halloysite nanotubes (HNTs) by adding the $CS(NH_2)_2$ solution into the $CdCl_2$ and HNTs suspension and then using hydrothermal treatment. The improved photocatalytic activity and stability of CdS/HNTs were attributed to the CdS nanoparticles which were uniformly dispersed on the surface of HNTs (Fig. 6). Ma *et al.*[92] adopted the hydrothermal method to prepare the TiO_2/hectorite composites with different Ti content. The composite with 2.5% Ti content has a larger specific surface area. Praus *et al.*[93] used the solution mixing method to prepare ZnS/montmorillonite composite by adding

montmorillonite into the ZnS nanodispersion and shaking for 24 h. Finally, the ZnS nanoparticles with average size of 5 nm were located on the montmorillonite external surface, blinding the micropores and mesopores of montmorillonite. In order to obtain the small and uniformly dispersed ZnS nanoparticles on the surface of montmorillonite, Kozák *et al*.[79] used cetyltrimethylammonium as a dispersant in the synthesis process of the ZnS/montmorillonite composite.

2.2 Surface and structure modifications of clay mineral-based photocatalysts

2.2.1 Hydrophobicity and hydrophilicity modification

Surface property of photocatalysts is an important factor for the photocatalytic degradation of low concentration liquid and gaseous organic pollutants.[94-96] In general, hydrophobicity property of the photocatalysts is in favor of improving their photocatalytic degradation for the organic pollutants. The hydrophobicity of the photocatalysts is usually controlled by the surface modification. Since the surface reaction sites for the hydrophobicity modification are not well-defined for photocatalysts, precisely controlled surface modification is not easily attained. For example, Nakato *et al*.[97] prepared the layered $K_4Nb_6O_{17}$ and adjusted its hydrophobicity with the intercalation of alkylammonium ions into the interlayer spaces to enable emulsification in a toluene-water system. Modification with dodecylammonium ions turned the $K_4Nb_6O_{17}$ catalyst more hydrophobic, and the catalyst were located not only at the toluene-water interface but also inside the toluene continuous phase. The obtained $K_4Nb_6O_{17}$ catalyst could effectively decompose the hydrophobic porphyrin and dye. Superhydrophobicity is that the surfaces with water contact angles higher than 150°. The superhydrophobic photocatalyst has attracted a great attention in the field of photocatalysis, shipbuilding, and other industries.[98-101] However, some photocatalysts with superhydrophobicity have disadvantageous influences in the photocatalytic processes. For example, Kim *et al.*[102] investigated that hydrophobic polydimethylsiloxane-coating on TiO_2 was highly stable and resistant toward photocatalytic degradation. Photocatalytic activity of TiO_2 was completely suppressed by the polydimethylsiloxane-coating, which was proven using toluene oxidation as a model reaction.

As for the clay mineral-based photocatalysts, the physical and chemical properties of clay supports strongly affect their photocatalytic properties. As reported by Lagaly and Ziesmer,[103] the concentration of the clay in water was related to the hydrophilicity of the clay and high concentration (more than 10%) clay in water dispersion may coagulate, limiting the concentration range of the clay to be used in aqueous dispersions. The clay supports can adsorb organic compounds on their external surfaces and within their interlayer spaces and lead to the higher concentration of dilute organic compounds around supported semiconductors in air or water. Clay minerals with relatively less hydrophilic surfaces should be a more effective photocatalyst supports for the elimination of hydrophobic organic pollutants[104, 105]. For example, Ooka *et al*.[104] used TiO_2 pillared clay for the adsorption and photocatalytic degradation of the endocrine disruptors with various hydrophobicities. From the results, the hydrophobicity of TiO_2 pillared clay was proposed as one of major factors in adsorption and photocatalytic degradation of the endocrine disruptor, which affected the enrichment of reactant and the efficiency of photodegradation. Rezala *et al*.[106] also found that the hydrophobic nature of TiO_2 pillared montmorillonite clays was beneficial for alkylaromatics to reach the photoactive sites. The hydrophobicity property of clay minerals is also good for the degradation of the gaseous pollutants. Kibanova, *et al*.[107] used TiO_2/kaolinite and TiO_2/hectorite composites for the elimination of toluene gas. The results suggested that competition of toluene gas with an excess of water on the surface of the composites was an important factor for the removal rate of toluene gas. However, it was also clarified that the use of the photocatalyst could not provide any advantage for less hydrophobic pollutants. To improve hydrophobicity of the catalyst supports, some organic solvent and surfactant were used in the synthesis process of the photocatalysts. Kuwahara *et al*.[108] successfully modified the surface properties of the supports by the post synthetic grafting of fluorine group containing silylation reagents, and quite effective improved the photocatalytic properties.

2.2.2 Acid treatment

Acid treatment has been widely used for the improvement of adsorption capability of clay minerals. During acid treatment, some of mineral impurities could be eliminated, and the interlayer cations are replaced by H^+ ions followed by dissolution of aluminum octahedral and silicon tetrahedral sheets and subsequent dissolution of structural cations. Octahedral cations such as Al^{3+}, Fe^{2+}, Fe^{3+} and Mg^{2+} can be removed by treating the clay minerals with acids at elevated temperatures. The removal rates of cations generally follow the order $Mg^{2+} > Fe^{2+} > Fe^{3+} > Al^{3+}$. The most important physical changes in acid-treated clays are the increase of their specific surface area and the average pore volume. Besides, the Brønsted and Lewis acid sites of clay minerals largely depend on the structural modifications caused by acid treatment. The pollutants are easy to contact the surface the clay minerals because the acid sites promote a strong interaction with them.[109-112] For example, Nguetnkam *et al*.[112] found that the acid treatment of Cameroonian clays leads to the partial destruction of the original clay structure, the formation of an amorphous silica, and the increase of the specific surface area and mesoporosity. Eloussaief and Benzina[113] used the sulphuric acid-treated clays for the adsorption of Pb and they have better adsorption capability than that of industrial silica gel and activated carbon. Auta and Hameed[114, 115] reported the acid-treated clay for adsorption of methylene blue. The acid-treated clay possesses better adsorption capacity than the raw clay due to the increase of the specific surface area. In fact, the photocatalytic properties of the semiconductor photocatalysts also can be influenced by the aid treatment.[116] For example, Wang *et al*.[117] considered that PO_4^{3-} and PO_4^{3-}/SO_4^{2-} increased the absorbance of TiO_2 in ultraviolet region and enhanced its photocatalytic activity distinctly. As for the clay mineral-based photocatalysts, the clay mineral supports with larger specific surface area and porous structures are beneficial to the improvement of their adsorption capability and the introduction of the semiconductor. With the increase of the amount of semiconductor in the clay mineral-based photocatalysts, more active sites can be formed on the surface of clay mineral supports. In particular, the porous structures provide lots of channels for the diffusion of pollutant molecules during the photocatalytic reaction. However, as we

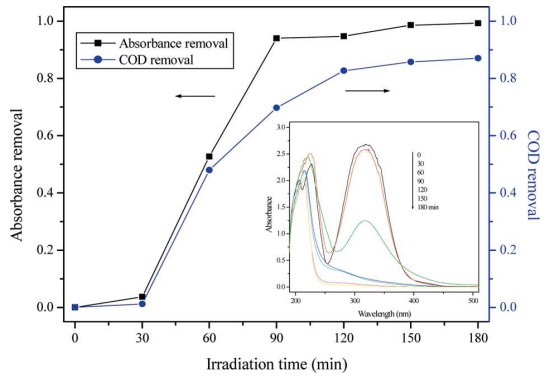

Fig. 7 Absorbance and COD removal of 4-NP. Inset: UV-visible spectral changes of 4-NP solution as a function of irradiation time. Adapted from ref. 125 with permission. Copyright 2010, American Chemical Society.

known, the acid treatment of the as-prepared clay mineral-based photocatalysts is not an effective way for the improvement of the photocatalytic properties. In other words, the acid treatment is only used for the pretreatment of single clay mineral or semiconductor.

2.3 Photocatalytic degradation of refractory pollutants

Based on the previous researches, the clay mineral-based photocatalysts are suitable materials for photocatalytic degradation of diluted refractory organic compounds compared to the pure semiconductor photocatalysts as shown in Table 1.

In order to meet the requirements of future environmental and energy technologies, a series of strategies are employed for the researches of clay mineral-based photocatalysts. For example, Fatimah *et al.*[123] used aluminum pillared montmorillonite as a porous support to obtain TiO_2-aluminum pillared clay photocatalyst with high thermal stability and photocatalytic activity for methylene blue degradation. Meshram *et al.*[73] employed ZnO pillared bentonite to remove the phenol from the simulated effluent under at lower flow rate. The batch experiments suggested that the removal of phenol follows first-order reaction kinetics and the degradation rate of phenol was more enhanced under basic conditions rather than acidic ones. As the visible-light photocatalysts, Bi_2O_3 and $Bi_5O_7NO_3$ semiconductiors also were combined with rectorite.[124] The prepared samples possessed strong adsorbility and exhibited high efficient photocatalytic activity for the degradation of Rhodamine B dye and 2,4-dichlorophenol under visible light irradiation. The excellent photocatalytic activity of Bi_2O_3/$Bi_5O_7NO_3$/rectorite was ascribed to its strong adsorption ability and the formation of Bi_2O_3/$Bi_5O_7NO_3$ heterojunction. Zhang *et al.*[125] synthesized Fe_2O_3 pillared rectorite by a solution mixing method and the prepared catalyst showed excellent photocatalytic activity for the degradation of 4-nitrophenol (4-NP), the results were shown in Fig. 7. From the Fig. 7, it can be seen that after degradation for 180 min, the absorbance and COD removal rate of 4-NP reached 99.3% and 87.0%, respectively.

Recent decade, silver/silver halide-based (Ag/AgX, X = Br, Cl, I) nanomaterials have been developed as photocatalysts and they display excellent plasmonic photocatalytic performance in the degradation of pollutants under visible light irradiation. However, most of plasmonic photocatalytsts display photocorrosion that can seriously deactivate photocatalysts in the photocatalysis

Table 1 The degradation activites of the clay mineral-based photocatalysts and the reference semiconductor photocatalysts.

Clay mineral-based photocatalyst	Pollutant type	Degradation activites	Reference semiconductor photocatalyst	Reference
TiO_2/Montmorillonite	Methylene blue	Removal rate was about 98% in 90 min	Removal rate is about 46% (Degussa, TiO_2)	88
TiO_2/Montmorillonite	Phenol	Mineralized carbon content (mg) is 420.1 in 120 min	Mineralized carbon content (mg) is 170.1 with TiO_2	118
TiO_2/Montmorillonite	Acid red G	Removal rate was about 98% in 120 min	Removal rate was about 76% with TiO_2	119
TiO_2/Bentonite	Cationic red GTL	Removal rate was about 90.1% in 240 min	Removal rate was about 58.7% with TiO_2	120
CdS/Halloysite	Tetracycline	Removal rate was about 93% in 60 min	Removal rate was about 73% with CdS	81
CdS/Montmorillonite	Methylene blue	Removal rate was about 92% in 180 min	Removal rate was about 16% with CdS	121
CdS/Rectorite	Rhodamine B	Removal rate was about 87% in 90 min	Removal rate was about 15% with CdS	122
Bi_2WO_6/Rectorite	4BS dye	Removal rate was about 98% in 120 min	Removal rate was about 91% with Bi_2WO_6	90

process and the underlying photocorrosion mechanism for the silver compounds is needed. It is widely accepted that the metallic Ag formed on the surface of AgX can separate electron-hole pairs by forming Schottky barrier, which not only enhances photocatalytic activity but also improves the photostability of AgX. The plasmonic oscillation of Ag NPs depends on their size and distribution, which determines the visible-light absorption of plasmonic photocatalysts. Micrometer-sized Ag/AgX particle causes the recombination of plasmon-induced electron-hole pairs before they arrive at the surface of photocatalyst, resulting in the loss of the efficiency of plasmonic photocatalytic system. Supported and composite Ag/AgX photocatalysts have been successfully used in pollutant degradation for exploring approaches to modulate the photon and charge carrier transport in photocatalysis system. Yang and zhang.[83] prepared the Ag/AgBr/attapulgite composite photocatalyst by a solution mixing method. The Ag/AgX particles with nanometer sizes are dispersed on the surface of clays. The plasmonic photocatalyst showed excellent photocatalytic activity and stability for the degradation of the Rhodamine B (RhB) pollutants and a possible mechanism was proposed (Fig. 8). Zhang *et al.*[126] synthesized Ag/AgBr/palygorskite with different bromine precursors. Compared to the AgBr/palygorskite composite synthesized with NaBr, the AgBr/palygorskite composite synthesized with $N(CH_2CH_2CH_2CH_3)_4Br$ showed an enhanced photocatayitc property owing to the smaller size of AgBr particles in AgBr/palygorskite. Quantum size effects and the suppressed

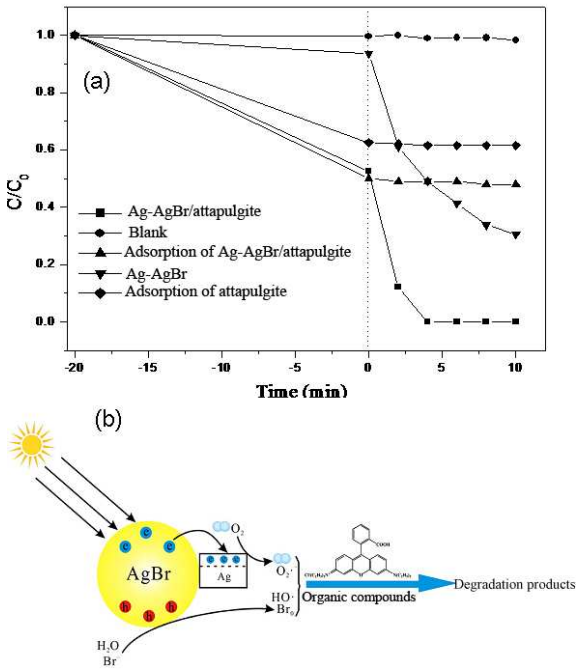

Fig. 8 The photodegradation efficiencies of RhB solution as a function of time under different conditions (a) and the possible mechanism (b). Adapted from ref. 83 with permission. Copyright 2012, Elsevier.

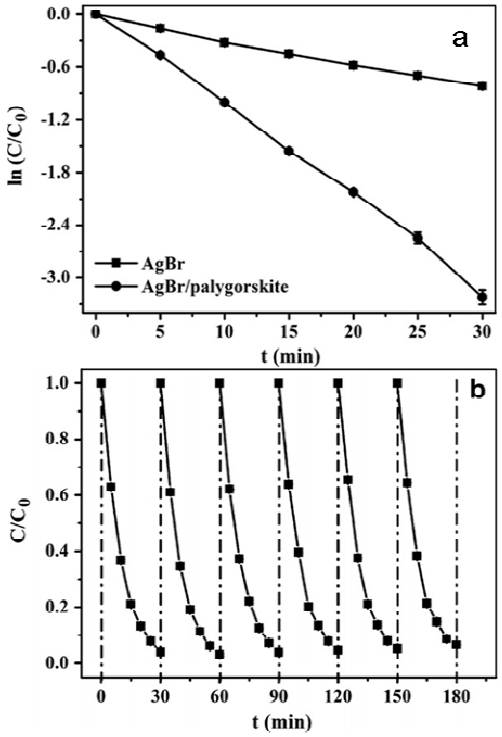

Fig. 9 (a) Effect of bromine precursors on photocatalytic performance. (b) Consecutive recycling dynamic curves over AgBr/palygorskite. Error bars represent standard deviations of triplicate measurements. Adapted from ref. 126 with permission. Copyright 2012, Elsevier.

recombination of electron-hole pairs were in favor of the improvement of photocatayitc property. After six cycles for RhB degradation under visible light irradiation, the AgBr/palygorskite composite did not exhibit obvious loss of photocatalytic activity, indicating its excellent photostability (Fig. 9).

For further explaining the role of clay minerals in the photocatalysis, we discuss the possible mechanisms in detail below. As the above reported papers, it can be concluded that the enhanced photocatalytic performances of clay-based photocatalysts are attributed to their large specific surface area and layer structures for the uniform load of the semiconductor photocatalysts, and high adsorption properties for the enrichment of low concentrated pollutants. However, in most cases, these clay minerals merely provide microenvironments for the photoreactions and they do not participate in the electron transfer reactions. In the past decade, researchers have made attempt to investigate the internal relationship between the clay minerals and semiconductor photocatalysts. Teng *et al.*[127] firstly reported that the montmorillonite K 10 could mediate the electron transfer via the contained electrochemically active iron species, which could form a high yield, long-lived photogenerated charge separation state. Miyamoto *et al.*[128, 129] found that the lifetime of the photogenerated charge separation state was increased dramatically in a colloidal mixture consisting of $K_4Nb_6O_{17}$ nanosheets and photochemically inert clay. The stability and efficiency of the charge separation are also controllable over a wide range of the contents of clay nanosheets. Subsequently, Ide *et al.*[130] reported the improved efficiency in the photocatalytic oxidation of aqueous benzene over TiO_2 in aqueous clay mineral suspension. The mineralization rate of benzene varied depending on the amounts and kinds of the added clays (saponite, montmorillonite and talc). It was important that the adsorption of the benzene on the saponite and talc hardly contributed to the benzene decomposition process. This fact is different from the mostly reported results that the adsorption property of clay minerals is beneficial to the photocatalytic degradation of pollutants. Although the some of minerals are directly participating in the photocatalytic reaction and improving the separation efficiency of photogenerated charge and hole, it is necessary to further investigate the photocatalytic mechanism for the degradation of pollutants over the clay-mineral photocatalysts, including the role of adsorption and the relationship between adsorption and photochemical reaction.

3 Synthesis and photocatalytic applications of LDH-based photocatalysts

3.1 Synthesis of LDH-based photocatalysts

Usually, LDHs are used as supports and combined with the semiconductors (e.g. SnO_2,[76] TiO_2,[131] ZnO,[132] CeO_2[133]). Besides, some of them could be directly used as photocatalysts (e.g. Zn-Al LDH,[134] Zn-Ti LDH,[135] Zn-Fe LDH,[136] Cu-Cr LDH,[137] Mg-Fe-Al LDH,[138]). There are several approaches to prepare synthetic LDH-based photocatalysts, including coprecipitation method, solution mixing method, template synthesis, hydrothermal method, ion exchange method, etc. More information about these methods is presented in the following sections.

3.1.1 Coprecipitation method

The simplest and most commonly used method for the preparation of LDHs is coprecipitation. In this method, aqueous solutions of divalent, trivalent and tetravalent cations containing the anion that is to be incorporated into the LDHs are used as precursors. In order to ensure simultaneous precipitation of two or more cations, it is necessary to carry out the synthesis under

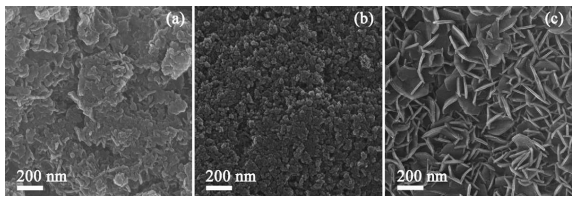

Fig. 10 SEM images of (a) CuMgAlTi-LDH, (b) CuMgAlTi-MMO, and (c) TiO_2/CuMgAl-RLDH. Adapted from ref. 131 with permission. Copyright 2012, Elsevier.

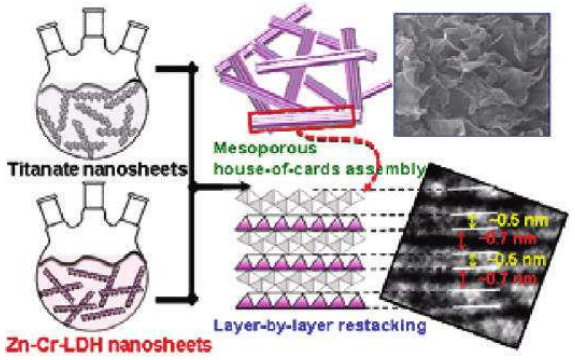

Fig. 11 Schematic illustration of the preparation of mesoporous layer-by-layer ordered nanohybrids of titanate/Zn-Cr LDH. Adapted from ref. 144 with permission. Copyright 2011, American Chemical Society.

conditions of supersaturation. After precipitation at supersaturation, an aging process is performed to increase the yields and crystallinity of the LDHs.[61] For example, Silva *et al*.[139] prepared the Zn-Cr LDH, Zn-Ti LDH and Zn-Ce LDH with NaOH and urea solution as precipitators, respectively. The hydrolysis of urea was very slowly which allowed for preparing material with a better crystallinity and an easy control of the particle size. Meanwhile, ternary LDHs with high photocatalytic properties have also been investigated. Mantilla *et al*.[140] prepared Zn-Al-Fe LDHs with different Zn:Al:Fe ratio and the results showed that Fe^{3+} in Zn-Al-Fe LDH played an important role in the photocatalytic properties. Huang *et al*.[141] firstly reported visible light driven Mg-Zn-In ternary LDHs by coprecipitation of $Mg(NO_3)_2{\cdot}6H_2O$, $Zn(NO_3)_2{\cdot}6H_2O$ and $InCl_3{\cdot}4H_2O$ solution in the alkaline conditions. As the increase of zinc content in Mg-Zn-In LDHs, the absorption edges of samples shifted toward visible region. As is well known that the calcinations can destroy the structure of LDH, but the calcined LDH is able to reconstruct the original structure when it is exposed to water and anions by the ''memory effect''.[142] Nowadays, the reconstruction function is widely used for the preparation of semiconductor/LDH composite photocatalysts. Lu *et al*.[131] successfully fabricated TiO_2 nanoparticle and reconstructed layered double hydroxide composite (TiO_2/CuMgAl-RLDH) by selective reconstruction of a Cu-Mg-Al-Ti LDH precursor, The preparation method mainly included the coprecipitation, calcination and rehydration processes. The SEM image of showed that the Cu-Mg-Al-Ti LDH precursor was made up of agglomerated platelet-shaped particles with average size of 20-50 nm (Fig. 10a). It should be mentioned that after calcination the lamellar LDH structure collapsed (Fig. 10b). Moreover, after rehydration, the LDH structure was regenerated (Fig. 9c).

3.1.2 Solution mixing method

Solution mixing has been widely used to fabricate semiconductor/LDH composite photocatalysts. For example, Valente *et al*.[133] prepared CeO_2/MgAl LDH composite photocatalyst by mixing the obtained Mg-Al LDH and cerium nitrate solution under vigorous mechanical stirring. A small amount of CeO_2 clusters were formed and uniformly distributed on the surface of the Mg-Al LDH.. Carja *et al*.[143] reported a novel bicomponent photoresponsive nanocomposite (TiO_2/ZnLDH) consisting of zinc-based anionic clay (ZnLDH) and TiO_2 nanoparticles which was obtained by the structural reconstruction of the ZnLDH in a $TiOSO_4$ aqueous solution. The reconstruction process of the ZnLDH in a $TiOSO_4$ aqueous medium had significant influences in the structure, texture, surface, and morphology features as compared to the ZnLDH. Gunjakar, *et al*.[144] synthesized the mesoporous layered TiO_2/Zn-Cr LDH composites by the mixing of the formamide suspensions of Zn-Cr-LDH and layered TiO_2 nanosheets under a constant stirring at room temperature in N_2 atmosphere (Fig. 11). Three kinds of mesoporous layered TiO_2/Zn-Cr LDH composites were synthesized by self-assembly between the oppositely charged nanosheets of Zn-Cr LDH and layered TiO_2 with the layered TiO_2/Zn-Cr LDH ratios of 0.91, 1.16 and 1.46. Similarly, Hadnadjev-Kostic *et al*.[145] mixed TiO_2 and thermally treated Zn-Al LDH in Na_2CO_3 solution to prepare the TiO_2/Zn-Al LDH nanocomposite photocatalyst. Carja *et al*.[146] fabricated CuO/LDH composite photocatalyst during the structural reconstruction of the layered LDH in the aqueous solution of $Cu(CH_3COO)_2$. The CuO nanoparticles with an average diameter of ca. 5-7 nm are well distributed on the larger particles (ca. 100 nm) of the LDH, forming the CuO-LDH heterojunctions.

3.1.3 Other methods

Besides the aforementioned methods, other synthesis methods of LDH photocatalysts included template synthesis, hydrothermal method, ion exchange method have been reported. For example, Zhao *et al*.[147] reported a curved and porous Zn-Al LDH photocatalyst through a biotemplated method. A uniform Al_2O_3 coating on the surface of the legume was fabricated through a low temperature atomic layer deposition process. In addition, the Zn-Al LDH film, which faithfully inherited the initial surface structure of the legume, was prepared by an in situ growth technique (Fig. 12). Dutta *et al*.[148] synthesized the highly crystalline Zn-Al LDH photocatalyst using hexamethylenetetramine as well as aluminum plate under the hydrothermal condition. Fan *et al*.[149] used a facile anion-exchange and light reduction method to synthesize bifunctional Ag/AgBr/Co-Ni-NO_3 LDH nanocomposite photocatalyst. Firstly, Co-Ni-Br LDH sheets were prepared by a topochemical synthesis method. Secondly, $AgNO_3$ solution was added to the suspension of Co-Ni-Br LDH sheets. Then Ag^+ reacted with the Br^- in the LDH interlayers and AgBr nanoparticles were formed on the surface of the LDH sheets, while Br^- entered in the LDH interlayers. Finally, Ag/AgBr nanoparticles with diameters of 50-150 nm were highly dispersed on the Co-Ni-NO_3 LDH sheets after light reduction (Fig. 13).

3.2 Photocatalytic degradation of refractory pollutants

It is well known that there has been considerable interest in the use of LDHs to remove anion species from solution. LDHs can directly remove the anion species from solution by three approaches which are surface adsorption, interlayer anion

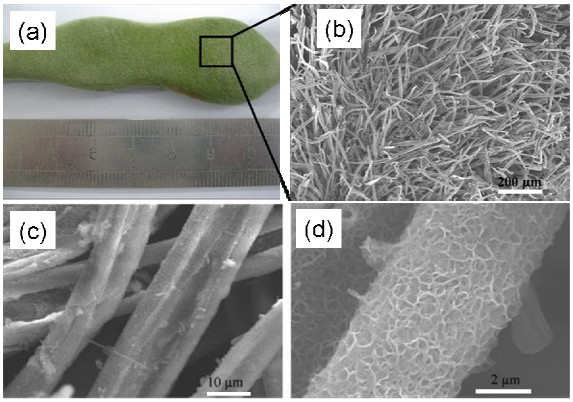

Fig. 12 (a) Optical photograph of the legume; (b) SEM images of the tubular trichome on the surface of the legume; (c,d) SEM images of the in situ growth LDH/legume film. Adapted from ref. 147 with permission. Copyright 2009, American Chemical Society.

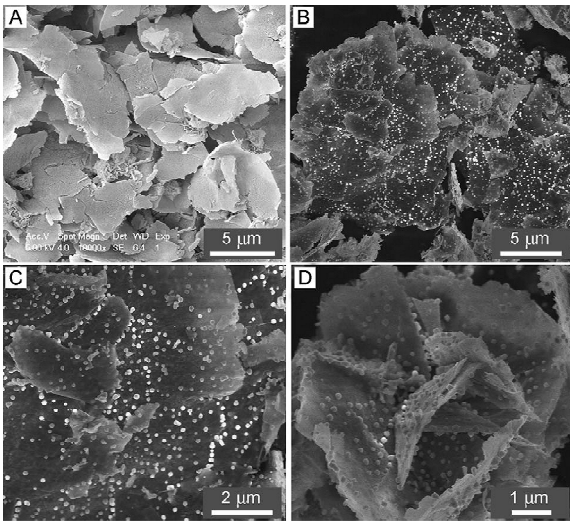

Fig. 13 (A) SEM image of Co-Ni-NO_3 LDH sheets. (B, C, D) SEM image of Ag/AgBr Co-Ni-NO_3 LDH nanocomposites. Adapted from ref. 149 with permission. Copyright 2013, Wiley-VCH.

exchange and reconstruction of the calcined LDHs. Recently, LDH-based photocatalysts have been widely applied for the photocatalytic degradation of organic compounds due to their large specific surface area, flexible interlayer space, abundant surface –OH and special structure units. By now, significant progresses have been achieved in the development of LDHs' application in environmental protection as shown in Table 2. From the Table 2, it can be concluded that the LDH-based photocatalysts have an enhanced photocatalytic activities as compared to the semiconductor photocatalysts.

The introduction of LDHs in LDH-based photocatalysts extended light absorption range and enhanced electron-transfer properties. For example, Carja *et al*.[143] employed TiO_2/LDH nanocomposite for phenol photodegradation. The obtained photocatalyst showed superior photocatalytic activity in comparison with Degussa P25. The excellent photocatalytic performances might arise from the specific nanotexture of the obtained nanocomposite self-assembly that can enhance the light harvesting and the favorable electron-transfer properties of the TiO_2/LDH heterojunctions. From the point of view of LDH structure, the surface of LDH is constituted by the –OH, which

Table 2 The degradation activites of the LDH-based photocatalysts and the reference semiconductor photocatalysts.

LDH-based photocatalyst	Pollutant type	Degradation activites	Reference semiconductor photocatalyst	Reference
TiO_2/Mg-Al LDH	Methyl orange	Removal rate was about 89% in 60 min	Removal rate was about 79% with P-25	150
TiO_2/Mg-Al-Ti LDH	Methyl orange	Removal rate was about 90% in 20 min	Removal rate is about 15% with P-25	150
CeO_2/Mg-Al LDH	Phenol	Removal rate was about 50% in 420 min	Removal rate was about 25% with P-25	133
Mg-Zn-In LDH	Methylene blue	Removal rate was about 80% in 120 min	Removal rate was about 35% with In_2O_3	141
Ag/AgBr/Co-Ni LDH	Methyl orange	Removal rate was about 100% in 120 min	Removal rate was about 63%, 15% with Ag/AgBr and Co-Ni-Br LDH, repectively	149
Ag_2WO_4/Zn-Cr LDH	Rhodamine B	Removal rate was about 100% in 100 min	Removal rate was about 15.8%, 13.2% with Ag_2WO_4 and Zn-Cr LDH, repectively	151

inhibit the organic pollutants to contact the LDH layer.[152] Therefore, surface modification approaches have been investigated for the improvement of the photocatalytic property of LDH-based photocatalysts. For example, Huang *et al*.[153] prepared the SDS-LDHs/TiO_2 composite by a hydrothermal method and the composite showed an enhanced adsorption after sodium dodecyl sulfate (SDS) modification. During the photodegradation of dimethyl phthalate (DMP), –OH on the surface of the composite played a key role in the photocatalytic degradation of pollutant molecule, which could be captured by h^+, consequently preventing the recombination of the h^+ and e^-. The photocatalytic degradation mechanism presented that the enrichment of DMP onto the SDS-LDHs/TiO_2 composite and the –OH the surface of the composite produced a synergistic effect, enhancing the photocatalytic degradation rate of DMP (Fig. 14).

LDHs as plasmonic photocatalyst supports have also been used for the photocatalysis. Fan *et al*.[149] synthesized bifunctional Ag/AgBr/Co-Ni-NO_3 LDH nanocomposites to adsorb and degrade organic pollutants in water. Without light illumination, the nanocomposites quickly adsorbed methyl orange, and the adsorptive capacity can reach 230 mg g^{-1}. The adsorption and photocatalytic properties of the nanocomposites for the removal of dyes and phenol were higher than those of Co-Ni-Br LDH and Ag/AgBr, which were attributed to the large specific surface area, highly dispersed Ag/AgBr nanoparticles and plenty of –OH on the surface of LDH nanocomposites. Nocchetti *et al*.[154] fabricated the Ag/AgCl/Zn-Al LDH nanocomposites by employing the Zn-Al LDH as a support. The Ag/AgCl/Zn-Al LDH nanocomposites showed a very good antimicrobial activity against both Gram positive and Gram negative bacteria and fungi. The antibacterial activity may be correlated with the release of the silver ions deriving both from silver chloride and from metallic silver NPs present on the LDH surface. The results indicated that the LDH surface not only acted as a support to anchor and grow AgCl nanoparticles (NPs) and Ag NPs, but played an important role in the stabilization of nanoparticles very likely through interactions between NPs and –OH.

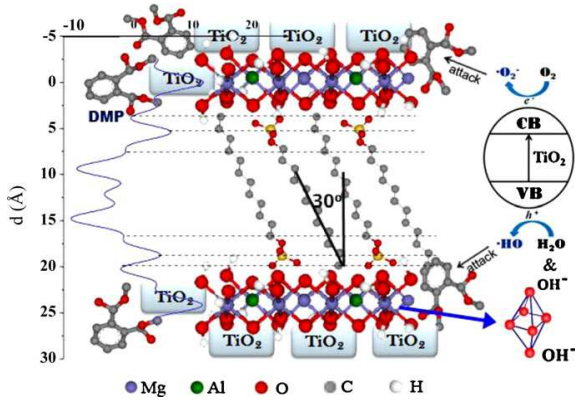

Fig. 14 Schematic representation of the adsorptive and photocatalytic degradation of DMP in presence of SDS-LDHs/TiO_2 composite. Adapted from ref. 153 with permission. Copyright 2013, Elsevier.

Although LDHs are well-known catalyst supports, they have seldom been used as photocatalysts several years ago. Recent years, some of LDHs show excellent photocatalytic activity for the degradation of organic compounds.[140, 155] For example, Mohapatra *et al.*[156] prepared Zn-Cr LDH by coprecipitation method and the LDH could effectively decompose the Rhodamine B, Rhodamine 6G and 4-chloro 2-nitro phenol pollutants under visible-light irradiation. Similarly, Chen *et al.*[157] fabricated Fe_3O_4/Zn-Cr LDH composite via hydrothermal method and investigated the adsorption capacity and photocatalytic activity of the composite for methylene blue dye removal. The Fe_3O_4 in composite provided the magnetic property of the composite, which improved the separation of the composite from aqueous solution. Parida *et al.*[158] prepared a series of Cu-Co/Cr ternary LDHs for the degradation of malachite green. When the Co/Cr = 0.1/0.067, the LDH photocatalyst exhibited high photocatalytic activity in the visible region due to the synergistic effect of binary cations and more electron-transfer capability of cobalt along with uniform pore size distribution.

According to the previously reported results, the possible mechanism for the quick and effective degradation of pollutant over the LDH-based and LDH photocatalysts was discussed. The adsorption capability and surface –OH of LDH are in favor of the enrichment of pollutants and separation of electron-hole pairs, improving the photocatalytic activity. The special morphologies and heterojunctions formed by these LDHs and semiconductor photocatalysts further enhance the light harvesting and separation of electron-hole pairs. As for some LDH photocatalysts, the MO_6 (e.g. M = Ti, Cr) octahedral units in LDH layer act as semiconductors. The electron transfer spectra from oxygen atoms of the lattice to the Ti^{4+} or Cr^{3+} ions lead to a more efficient electron separation with the formation of electron-hole pairs.[139] The e^- and h^+ can react with water and dissolved oxygen on the surface of the LDH photocatalyst to form hydroxyl radicals ($^{\bullet}OH$) and superoxide radicals ($^{\bullet}O_2^-$), respectively, which are highly oxidizing species. The possible reaction processes for photocatalytic degradation of pollutant with the LDH were summarized by the following eqn (1-8).[158]

$$LDH + h\nu \rightarrow h^+ + e^- \quad (1)$$

$$h^+ + H_2O \rightarrow 2H^+ + 2\,^{\bullet}OH \quad (2)$$

$$e^- + O_2 \rightarrow {}^{\bullet}O_2^- \quad (3)$$

$$^{\bullet}O_2^- + H^+ \rightarrow HO_2^{\bullet} \quad (4)$$

$$HO_2^{\bullet} + HO_2^{\bullet} \rightarrow H_2O_2 + O_2 \quad (5)$$

$$H_2O_2 \rightarrow 2\,^{\bullet}OH \quad (6)$$

$$^{\bullet}O_2^- + \text{pollutants} \rightarrow \text{degradation products} \quad (7)$$

$$^{\bullet}OH + \text{pollutants} \rightarrow \text{degradation products} \quad (8)$$

It is well known that the quantum size effect of the semiconductor photocatalysts affects the photocatalytic activities.[37, 159-161] Similarly, the crystal size of LDHs is related to their photocatalytic activities as shown in Table 3. From the Table 3, it can be seen that small crystal size of LDHs facilitates the improvement of photocatalytic activities, which can effectively inhibit the recombination between e^- and h^+.

Table 3 The crystallite sizes of LDHs and their photocatalytic activities.

Catalyst	Crystallite size (nm)	Pollutant	Pollutant degradation rate (%)	Reference
Zn-Fe-CO_3 LDH	28	Methyl violet/ Malachite green	99/98.5	127
Zn-Fe-Cl LDH	29	Methyl violet/ Malachite green	75/72	127
Zn-Fe-NO_3 LDH	31	Methyl violet/ Malachite green	66/64	127
Zn-Ti-NO_3 LDH	35	Rhodamine B	98	162
Zn-Al-NO_3 LDH	33	Rhodamine B	96	162
Zn-Fe-Ti-NO_3 LDH	47	Rhodamine B	88	162
Zn-Fe-NO_3 LDH	69	Rhodamine B	72	162

3.3 Photocatalytic H_2 generation and reduction of CO_2

A variety of semiconductor photocatalysts such as MoS_2/CdS,[163] Co_3O_4,[164] Ga_2O_3,[165, 166] $SrTiO_3$,[167, 168] Ta_3N_5,[169] $ZnIn_2S_4$,[170-172] TiO_2,[173-177] Zn_2GeO_4,[178] WO_3,[179, 180] $ZnGa_2O_4$,[181] have been investigated for photocatalytic H_2 generation and reduction of CO_2. However, the practical applications of this strategy are limited due to the low yield. Therefore, it is necessary to develop novel and efficient photocatalysts. Zhao *et al.*[182] prepared highly dispersed TiO_6 units in several LDHs which displayed a photocatalytic H_2-production rate of 31.4 $\mu mol \cdot h^{-1}$ as well as excellent recyclable performance. The existence of the TiO_6 units resulted in abundant surface defects that serve as trapping sites for photogenerated electrons. Parida *et al.*[183] reported that Fe-doped Mg-Al LDHs showed a good photocatalytic activity for H_2 generation under visible light irradiation using methanol as a sacrificial reagent. Various factors were also discussed for the explanation of the photocatalytic activity. On one hand, the incorporation of Fe^{3+} into Mg-Al LDH structure formed the $Fe(OH)_6$ octahedral units, shifted the light absorbance range and made it active for visible light photocatalysis. On the other hand, amount of Fe^{3+} in the Mg-Al LDHs and –OH in the LDH surface prevented the recombination of e^- and h^+, improving the photocatalytic activity. Very recently, Baliarsingh *et al.*[184] also prepared Ni-Zn-Cr LDHs for H_2 generation and discussed the

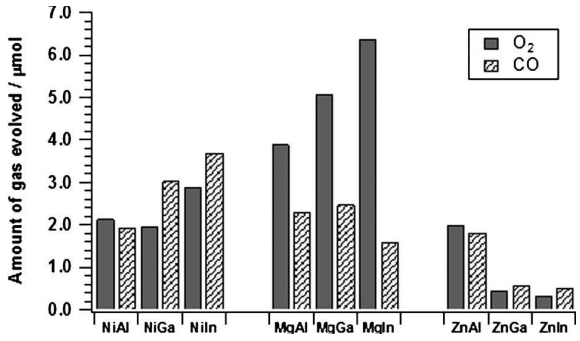

Fig. 15 Yields of O_2 and CO for the photocatalytic conversion of CO_2 in water, over various LDHs (M^{2+}/M^{3+} = 3) after 10 h of photoirradiation (light intensity is adjusted constantly). Adapted from ref. 187 with permission. Copyright 2012, Wiley-VCH.

detailed mechanism for H_2 generation. The enhanced photocatalytic activity of Ni-Zn-Cr LDHs was mainly attributed to the special structure, narrow band gap and large surface area. Ahmed *et al*.[185, 186] synthesized the Zn-Cu-M(III) (M = Al, Ga) LDHs and then applied the LDHs to convert gaseous CO_2 to methanol or CO under UV-visible light using hydrogen as a reductant. $[Zn_3Al(OH)_8]_2^+(CO_3)^{2-}\cdot mH_2O$ was the most active, producing CO with 94 mol% selectivity (0.16% conversion). $[Zn_{1.5}Cu_{1.5}Ga(OH)_8]_2^+(CO_3)^{2-}\cdot mH_2O$ was the most selective for producing methanol (68 mol%) at 0.03% conversion. The introduction of Cu sites in the LDH improved the methanol selectivity, which was attributed to be the binding of CO_2 at the Cu sites as hydrogen carbonate species Cu-O(-Zn)-C(OH)=O and Cu-O(-Ga)-C(OH)=O. Besides, the interlayer space in the LDH was in favor of the diffusion of CO_2 to the Cu sites. Teramura *et al*.[187] synthesized a series of LDHs with a M^{2+}/M^{3+} ratio of 3 (M^{2+} = Mg^{2+}, Zn^{2+}, Ni^{2+}; M^{3+} = Al^{3+}, Ga^{3+}, In^{3+}). The photocatalytic activities of the M^{2+}-M^{3+} LDHs for the conversion of CO_2 in water were showed in Fig. 15. The results indicated that the LDHs showed superior activity and the oxidation and reduction processes were listed by the following eqn (9-10).

$$CO_2 + 2\,e^- + 2\,H^+ \rightarrow CO + H_2O \quad (9)$$

$$2\,H_2O \rightarrow O_2 + 4\,H^+ + 4\,e^- \quad (10)$$

4 Conclusions and perspectives

As it has been stated in this review, a variety of synthesis methods such as sol-gel, solution mixing, coprecipitation approaches have been adopted for fabricating the clay-based photocatalysts. These composite photocatalysts have been widely used for the photocatalytic degradation of pollutants, H_2 generation and reduction of CO_2. This progress has demonstrated that clay-based photocatalysts are playing and will continue to play an important role in the environment protection and in the search for energy.

The photocatalytic mechanism during the photodegradation process with clay-based photocatalysts was also revealed: (1) High adsorption capabilities and surface hydrophobicity of clay materials enrich the concentration of pollutants on the surface of clay-based photocatalysts, accelerating the photocatalytic reaction rate. (2) Some clay materials can participate in the photochemical reaction by their structure units and surface –OH, which improve the light absorption range and electron and hole separation properties of the clay-based photocatalysts, then enhancing the photocatalytic activity and photostability.

It is worthy to further study the effects of the compositions and structures of the clays on the microstructure formation and the photocatalytic mechanisms of the clay-based photocatalysts. Different clay materials possesses different compositions and structure, resulting in the changes of adsorption capability, surface characteristics, microstructure, light absorption property, etc. and having an impact on the photocatalytic process. Therefore, it is necessary to study the intrinsic relation between the semiconductors and clay materials for the photocatalytic reaction. Especially, the study about the roles of the clay materials for the electron transportation and light absorption is very challenging and significant.

Acknowledgments

This work was supported by the National Basic Research Program of China (2013CB632402), National Key Technology R&D Program of China (2012BAJ25B02-03), Specialized Research Fund for the Doctoral Program of Higher Education (20110143110015), the Fundamental Research Funds for the Central Universities and Self-determined and Innovative Research Funds of "WUT" (2013-YB-007).

Notes and references

[a] *School of Resources and Environmental Engineering, Wuhan University of Technology, Wuhan, 430070, P. R. China; Tel: 86-27-87651816; fax: 86-27-87887445; E-mail: gkzhang@whut.edu.cn; zgkwu@126.com*
[b] *State Key Laboratory of Silicate Materials for Architectures, Wuhan University of Technology, Wuhan 430070, P. R. China*

1 J. Bujdák, *Appl. Clay Sci.*, 2006, **34**, 58-73.
2 S. Navalon, M. Alvaro and H. Garcia, *Appl. Catal. B: Environ.*, 2010, **99**, 1-26.
3 G. S. Li, D. Q. Zhang and J. C. Yu, *Environ. Sci. Technol.*, 2009, **43**, 7079-7085.
4 N. Q. Wu, J. Wang, D. N. Tafen, H. Wang, J. G. Zheng, J. P. Lewis, X. G. Liu, S. S. Leonard and A. Manivannan, *J. Am. Chem. Soc.*, 2010, **132**, 6679-6685.
5 R. Leary and A. Westwood, *Carbon*, 2011, **49**, 741-772.
6 S. Hoang, S. Guo, N. T. Hahn, A. J. Bard and C. B. Mullins, *Nano Lett.*, 2012, **12**, 26-32.
7 F. Lu, W. P. Cai and Y. G. Zhang, *Adv. Funct. Mater.*, 2008, **18**, 1047-1056.
8 D. D. Lin, H. Wu, R. Zhang and W. Pan, *Chem. Mater.*, 2009, **21**, 3479-3484.
9 G. K. Zhang, X. Shen and Y. Q. Yang, *J. Phys. Chem. C*, 2011, **115**, 7145-7152.
10 C. Y. Wang, H. Zhang, F. Li and L. Y. Zhu, *Environ. Sci. Technol.*, 2010, **44**, 6843-6848.
11 E. P. Gao, W. Z. Wang, M. Shang and J. H. Xu, *Phys. Chem. Chem. Phys.*, 2011, **13**, 2887-2893.
12 Z. J. Zhang, W. Z. Wang, E. P. Gao, S. M. Sun and L. Zhang, *J. Phys. Chem. C*, 2012, **116**, 25898-25903.
13 S. M. Sun, W. Z. Wang and L. Zhang, *J. Phys. Chem. C*, 2013, **117**, 9113-9120.
14 S. L. Xiong, B. J. Xi and Y. T. Qian, *J. Phys. Chem. C*, 2010, **114**, 14029-14035.
15 L. Jia, D. H. Wang, Y. X. Huang, A. W. Xu and H. Q. Yu, *J. Phys. Chem. C*, 2011, **115**, 11466-11473.
16 X. J. Liu, L. K. Pan, T. Lv, G. Zhu, Z. Sun and C. Q. Sun, *Chem. Commun.*, 2011, **47**, 11984-11986.
17 Q. J. Xiang, B. Cheng and J. G. Yu, *Appl. Catal. B: Environ.*, 2013, **138**, 299-303.

18 G. K. Zhang, J. L. Yang, S. M. Zhang, Q. Xiong, B. B. Huang, J. T. Wang and W. Q. Gong, *J. Hazard. Mater.*, 2009, **172**, 986-992.
19 Z. H. Ai, W. K. Ho and S. Lee, *Appl. Surf. Sci.*, 2012, **263**, 266-272.
20 J. G. Hou, Z. Wang, S. Q. Jiao and H. M. Zhu, *CrystEngComm*, 2012, **14**, 5923-5928.
21 H. H. Gan, G. K. Zhang and H. X. Huang, *J. Hazard. Mater.*, 2013, **250**, 131-137.
22 J. H. Huang, K. N. Ding, Y. D. Hou, X. C. Wang and X. Z. Fu, *ChemSusChem*, 2008, **1**, 1011-1019.
23 S. C. Yan, L. J. Wan, Z. S. Li and Z. G. Zou, *Chem. Commun.*, 2011, **47**, 5632-5634.
24 J. Liu and G. K. Zhang, *CrystEngComm*, 2013, **15**, 382-389.
25 J. Liu, G. K. Zhang, J. C. Yu and Y. D. Guo, *Dalton Trans.*, 2013, **42**, 5092-5099.
26 P. Wang, B. B. Huang, X. Y. Qin, X. Y. Zhang, Y. Dai, J. Y. Wei and M. H. Whangbo, *Angew. Chem. Int. Ed.*, 2008, **47**, 7931-7933.
27 B. Ma, J. F. Guo, W. L. Dai and K. N. Fan, *Appl. Catal. B: Environ.*, 2013, **130-131**, 257-263.
28 M. Matsuoka, M. Kitano, M. Takeuchi, K. Tsujimaru, M. Anpo and J. M. Thomas, *Catal. Today*, 2007, **122**, 51-61.
29 M. Ni, M. K. H. Leung, D. Y. C. Leung and K. Sumathy, *Renew. Sust. Energ. Rev.*, 2007, **11**, 401-425.
30 X. B. Chen, S. H. Shen, L. J. Guo and S. S. Mao, *Chem. Rev.*, 2010, **110**, 6503-6570.
31 Y. H. Hu, *Angew. Chem. Int. Ed.*, 2012, **51**, 12410-12412.
32 C. S. Song, *Catal. Today*, 2006, **115**, 2-32.
33 H. Takeda and O. Ishitani, *Coord. Chem. Rev.*, 2010, **254**, 346-354.
34 S. C. Roy, O. K. Varghese, M. Paulose and C. A. Grimes, *ACS Nano*, 2010, **4**, 1259-1278.
35 Y. Izumi, *Coord. Chem. Rev.*, 2013, **257**, 171-186.
36 M. R. Hoffmann, S. T. Martin, W. Choi and D. W. Bahnemann, *Chem. Rev.*, 1995, **95**, 69-96.
37 A. Hagfeldt and M. Graetzel, *Chem. Rev.*, 1995, **95**, 49-68.
38 H. Tong, S. X. Ouyang, Y. P. Bi, N. Umezawa, M. Oshikiri and J. H. Ye, *Adv. Mater.*, 2012, **24**, 229-251.
39 X. W. Lou, L. A. Archer and Z. C. Yang, *Adv. Mater.*, 2008, **20**, 3987-4019.
40 W. C. Huang, L. M. Lyu, Y. C. Yang and M. H. Huang, *J. Am. Chem. Soc.*, 2012, **134**, 1261-1267.
41 M. Mrowetz, W. Balcerski, A. J. Colussi and M. R. Hoffmann, *J. Phys. Chem. B*, 2004, **108**, 17269-17273.
42 J. H. Park, S. Kim and A. J. Bard, *Nano Lett*, 2006, **6**, 24-28.
43 D. Dvoranova, V. Brezova, M. Mazur and M. A. Malati, *Appl. Catal. B: Environ.*, 2002, **37**, 91-105.
44 J. F. Zhu, Z. G. Deng, F. Chen, J. L. Zhang, H. J. Chen, M. Anpo, J. Z. Huang and L. Z. Zhang, *Appl. Catal. B: Environ.*, 2006, **62**, 329-335.
45 T. Hirakawa and P. V. Kamat, *J. Am. Chem. Soc.*, 2005, **127**, 3928-3934.
46 H. Choi, E. Stathatos and D. D. Dionysiou, *Appl. Catal. B: Environ.*, 2006, **63**, 60-67.
47 Y. Yao, G. Li, S. Ciston, R. M. Lueptow and K. A. Gray, *Environ. Sci. Technol.*, 2008, **42**, 4952-4957.
48 Y. H. Zhang, Z. R. Tang, X. Z. Fu and Y. J. Xu, *ACS Nano*, 2010, **4**, 7303-7314.
49 Y. D. Guo, G. K. Zhang, H. H. Gan and Y. L. Zhang, *Dalton Trans.*, 2012, **41**, 12697-12703.
50 Y. D. Guo, G. K. Zhang, J. Liu and Y. L. Zhang, *RSC Adv.*, 2013, **3**, 2963-2970.
51 J. L. Gunjakar, I. Y. Kim, J. M. Lee, N. S. Lee and S. J. Hwang, *Energ. Environ. Sci.*, 2013, **6**, 1008-1017.
52 J. Bujdák, *Applied Clay Science*, 2006, **34**, 58-73.
53 S. Navalon, M. Alvaro and H. Garcia, *Appl. Catal. B: Environ.*, 2010, **99**, 1-26.
54 C. H. Zhou, *Appl. Clay Sci.*, 2011, **53**, 87-96.
55 S. Ng and J. Plank, *Cem. Concr. Res.*, 2012, **42**, 847-854.
56 H. Shindo, D. Watanabe, T. Onaga, M. Urakawa, O. Nakahara and Q. Y. Huang, *Soil Sci. Plant Nutr.*, 2002, **48**, 763-767.
57 M. Z. Liu and H. M. Yang, *Appl. Clay Sci.*, 2010, **50**, 554-559.
58 X. He, A. D. Tang, H. M. Yang and J. Ouyang, *Appl. Clay Sci.*, 2011, **53**, 80-84.
59 B. Paul, W. N. Martens and R. L. Frost, *Appl. Clay Sci.*, 2012, **57**, 49-54.
60 V. Rives and M. Angeles Ulibarri, *Coord. Chem. Rev.*, 1999, **181**, 61-120.
61 K. H. Goh, T. T. Lim and Z. L. Dong, *Water Res.*, 2008, **42**, 1343-1368.
62 A. I. Khan and D. O'Hare, *J. Mater. Chem.*, 2002, **12**, 3191-3198.
63 D. G. Evans and X. Duan, *Chem. Commun.*, 2006, 485-496.
64 Z. P. Xu, J. Zhang, M. O. Adebajo, H. Zhang and C. H. Zhou, *Appl. Clay Sci.*, 2011, **53**, 139-150.
65 Q. Wang and D. O'Hare, *Chem. Rev.*, 2012, **112**, 4124-4155.
66 V. Rives, M. del Arco and C. Martin, *J. Controlled Release*, 2013, **169**, 28-39.
67 F. Cavani, F. Trifirò and A. Vaccari, *Catal. Today*, 1991, **11**, 173-301.
68 F. Leroux and J. P. Besse, *Chem. Mater.*, 2001, **13**, 3507-3515.
69 G. R. Williams and D. O'Hare, *J. Mater. Chem.*, 2006, **16**, 3065-3074.
70 V. Belessi, D. Lambropoulou, I. Konstantinou, A. Katsoulidis, P. Pomonis, D. Petridis and T. Albanis, *Appl. Catal. B: Environ.*, 2007, **73**, 292-299.
71 Y. L. Zhang, D. J. Wang and G. K. Zhang, *Chem. Eng. J.*, 2011, **173**, 1-10.
72 Y. L. Zhang, H. H. Gan and G. K. Zhang, *Chem. Eng. J.*, 2011, **172**, 936-943.
73 S. Meshram, R. Limaye, S. Ghodke, S. Nigam, S. Sonawane and R. Chikate, *Chem. Eng. J.*, 2011, **172**, 1008-1015.
74 R. Kun, M. Balázs and I. Dékány, *Colloids Surf., A*, 2005, **265**, 155-162.
75 S. P. Paredes, M. A. Valenzuela, G. Fetter and S. O. Flores, *J. Phys. Chem. Solids*, 2011, **72**, 914-919.
76 E. Dvininov, M. Ignat, P. Barvinschi, M. A. Smithers and E. Popovici, *J. Hazard. Mater.*, 2010, **177**, 150-158.
77 G. K. Zhang, X. M. Ding, F. S. He, X. Y. Yu, J. Zhou, Y. J. Hu and J. W. Xie, *Langmuir*, 2008, **24**, 1026-1030.
78 G. K. Zhang, X. M. Ding, Y. J. Hu, B. B. Huang, X. Y. Zhang, X. Y. Qin, J. Zhou and J. W. Xie, *J. Phys. Chem. C*, 2008, **112**, 17994-17997.
79 O. Kozak, P. Praus, K. Koci and M. Klementova, *J. Colloid Interface Sci.*, 2010, **352**, 244-251.
80 J. R. Xiao, T. Y. Peng, D. N. Ke, L. Zan and Z. H. Peng, *Phys. Chem. Miner.*, 2007, **34**, 275-285.
81 W. N. Xing, L. Ni, P. W. Huo, Z. Y. Lu, X. L. Liu, Y. Y. Luo and Y. S. Yan, *Appl. Surf. Sci.*, 2012, **259**, 698-704.
82 Y. Q. Yang, G. K. Zhang and W. Xu, *J. Colloid Interface Sci.*, 2012, **376**, 217-223.
83 Y. Q. Yang and G. K. Zhang, *Appl. Clay Sci.*, 2012, **67**, 11-17.
84 Z. Ding, J. T. Kloprogge, R. L. Frost, G. Q. Lu and H. Y. Zhu, *J. Porous Mater.*, 2001, **8**, 273-293.
85 Z. Ding, H. Y. Zhu, G. Q. Lu and P. F. Greenfield, *J. Colloid Interface Sci.*, 1999, **209**, 193-199.
86 M. Lim, Y. Zhou, B. Wood, L. Z. Wang, V. Rudolph and G. Q. Lu, *Environ. Sci. Technol.*, 2008, **43**, 538-543.
87 J. Y. Chen, X. L. Liu, G. Y. Li, X. Nie, T. C. An, S. Q. Zhang and H. J. Zhao, *Catal. Today*, 2011, **164**, 364-369.
88 D. M. Chen, Q. Zhu, F. S. Zhou, X. T. Deng and F. T. Li, *J. Hazard. Mater.*, 2012, **235**, 186-193.
89 G. Zhang, X. Ding, F. He, X. Yu, J. Zhou, Y. Hu and J. Xie, *J. Phys. Chem. Solids*, 2008, **69**, 1102-1106.
90 Y. D. Guo, G. K. Zhang and H. H. Gan, *J. Colloid Interface Sci.*, 2012, **369**, 323-329.
91 I. Fatimah, S. B. Wang and D. Wulandari, *Appl. Clay Sci.*, 2011, **53**, 553-560.
92 J. Ma, Y. Z. Jia, Y. Jing, J. H. Sun and Y. Yao, *Appl. Clay Sci.*, 2009, **46**, 114-116.
93 P. Praus, M. Reli, K. Koci and L. Obalova, *Appl. Surf. Sci.*, 2013, **275**, 369-373.
94 Y. Kuwahara, T. Kamegawa, K. Mori and H. Yamashita, *Chem. Commun.*, 2008, 4783-4785.
95 G. F. Guo, Y. Hu, S. M. Jiang and C. H. Wei, *J. Hazard. Mater.*, 2012, **223-224**, 39-45.

96 Y. Kuwahara and H. Yamashita, *J. Mater. Chem.*, 2011, **21**, 2407-2416.
97 T. Nakato, H. Ueda, S. Hashimoto, R. Terao, M. Kameyama and E. Mouri, *ACS Appl. Mater. Interfaces*, 2012, **4**, 4338-4347.
98 T. Kamegawa, Y. Shimizu and H. Yamashita, *Adv. Mater.*, 2012, **24**, 3697-3700.
99 C. R. Crick, J. C. Bear, A. Kafizas and I. P. Parkin, *Adv. Mater.*, 2012, **24**, 3505-3508.
100 M. Y. Xing, D. Y. Qi, J. L. Zhang, F. Chen, B. Z. Tian, S. Bagwas and M. Anpo, *J. Catal.*, 2012, **294**, 37-46.
101 S. Anandan, T. N. Rao, M. Sathish, D. Rangappa, I. Honma and M. Miyauchi, *ACS Appl. Mater. Interfaces*, 2013, **5**, 207-212.
102 K. D. Kim, H. O. Seo, C. W. Sim, M. G. Jeong, Y. D. Kim and D. C. Lim, *Prog. Org. Coat.*, 2013, **76**, 596-600.
103 G. Lagaly and S. Ziesmer, *Adv. Colloid Interface Sci.*, 2003, **100**, 105-128.
104 C. Ooka, H. Yoshida, M. Horio, K. Suzuki and T. Hattori, *Appl. Catal. B: Environ.*, 2003, **41**, 313-321.
105 C. Ooka, H. Yoshida, K. Suzuki and T. Hattori, *Appl. Catal. A: Gen.*, 2004, **260**, 47-53.
106 H. Rezala, H. Khalaf, J. L. Valverde, A. Romero, A. Molinari and A. Maldotti, *Appl. Catal. A: Gen.*, 2009, **352**, 234-242.
107 D. Kibanova, J. Cervini-Silva and H. Destaillats, *Environ. Sci. Technol.*, 2009, **43**, 1500-1506.
108 Y. Kuwahara, K. Maki, Y. Matsumura, T. Kamegawa, K. Mori and H. Yamashita, *J. Phys. Chem. C*, 2009, **113**, 1552-1559.
109 A. Gil, L. M. Gandia and M. A. Vicente, *Cat. Rev.*, 2000, **42**, 145-212.
110 T. Novaković, L. Rožić, S. Petrović and A. Rosić, *Chem. Eng. J.*, 2008, **137**, 436-442.
111 X. L. Guo, Y. D. Yao, G. F. Yin, Y. Q. Kang, Y. Luo and L. Zhuo, *Appl. Clay Sci.*, 2008, **40**, 20-26.
112 J. P. Nguetnkam, R. Kamga, F. Villiéras, G. E. Ekodeck, A. Razafitianamaharavo and J. Yvon, *Appl. Clay Sci.*, 2011, **52**, 122-132.
113 M. Eloussaief and M. Benzina, *J. Hazard. Mater.*, 2010, **178**, 753-757.
114 M. Auta and B. H. Hameed, *Chem. Eng. J.*, 2012, **198**, 219-227.
115 M. Auta and B. H. Hameed, *J. Ind. Eng. Chem.*, 2013, **19**, 1153-1161.
116 X. Z. Fu, W. A. Zeltner, Q. Yang and M. A. Anderson, *J. Catal.*, 1997, **168**, 482-490.
117 Z. C. Wang and H. F. Shui, *J. Mol. Catal. A: Chem.*, 2007, **263**, 20-25.
118 R. Kun, K. Mogyorosi and I. Dekany, *Appl. Clay Sci.*, 2006, **32**, 99-110.
119 Y. L. Zhang, L. J. Deng, G. K. Zhang and H. H. Gan, *Colloids Surf., A*, 2011, **384**, 137-144.
120 Z. S. Sun, Y. X. Chen, Q. Ke, Y. Yang and J. Yuan, *J. Photochem. Photobiol., A*, 2002, **149**, 169-174.
121 H. Boukhatem, L. Djouadi, N. Abdelaziz and H. Khalaf, *Appl. Clay Sci.*, 2013, **72**, 44-48.
122 J. R. Xiao, T. Y. Peng, K. Dai, L. Zan and Z. H. Peng, *J. Solid State Chem.*, 2007, **180**, 3188-3195.
123 I. Fatimah, S. B. Wang, Narsito and K. Wijaya, *Appl. Clay Sci.*, 2010, **50**, 588-593.
124 S. X. Wu, J. Z. Fang, W. C. Xu and C. P. Cenb, *J. Mol. Catal. A: Chem.*, 2013, **373**, 114-120.
125 G. K. Zhang, Y. Y. Gao, Y. L. Zhang and Y. D. Guo, *Environ. Sci. Technol.*, 2010, **44**, 6384-6389.
126 X. J. Zhang, J. L. Li, X. Lu, C. Q. Tang and G. X. Lu, *J. Colloid Interface Sci.*, 2012, **377**, 277-283.
127 Y. W. Teng, I. J. Chang and C. M. Wang, *J. Phys. Chem. B*, 1997, **101**, 10386-10389.
128 N. Miyamoto, Y. Yamada, S. Koizumi and T. Nakato, *Angew. Chem. Int. Ed.*, 2007, **46**, 4123-4127.
129 T. Nakato, Y. Yamada and N. Miyamoto, *J. Phys. Chem. B*, 2009, **113**, 1323-1331.
130 Y. Ide, M. Matsuoka and M. Ogawa, *ChemCatChem*, 2012, **4**, 628-630.
131 R. J. Lu, X. Xu, J. P. Chang, Y. Zhu, S. L. Xu and F. Z. Zhang, *Appl. Catal. B: Environ.*, 2012, **111**, 389-396.
132 Y. Zhi, Y. G. Li, Q. H. Zhang and H. Z. Wang, *Langmuir*, 2010, **26**, 15546-15553.
133 J. S. Valente, F. Tzompantzi and J. Prince, *Appl. Catal. B: Environ.*, 2011, **102**, 276-285.
134 E. M. Seftel, E. Popovici, M. Mertens, K. D. Witte, G. V. Tendeloo, P. Cool and E. F. Vansant, *Microporous Mesoporous Mater.*, 2008, **113**, 296-304.
135 M. F. Shao, J. B. Han, M. Wei, D. G. Evans and X. Duan, *Chem. Eng. J.*, 2011, **168**, 519-524.
136 K. M. Parida and L. Mohapatra, *Chem. Eng. J.*, 2012, **179**, 131-139.
137 L. Tian, Y. F. Zhao, S. He, M. Wei and X. Duan, *Chem. Eng. J.*, 2012, **184**, 261-267.
138 G. Carja, E. Husanu, C. Gherasim and H. Iovu, *Appl. Catal. B: Environ.*, 2011, **107**, 253-259.
139 C. G. Silva, Y. Bouizi, V. Fornés and H. García, *J. Am. Chem. Soc.*, 2009, **131**, 13833-13839.
140 A. Mantilla, F. Tzompantzi, J. L. Fernandez, J. A. I. Diaz Góngora, G. Mendoza and R. Gomez, *Catal. Today*, 2009, **148**, 119-123.
141 L. Huang, S. Chu, J. Q. Wang, F. Kong, L. L. Luo, Y. Wang and Z. G. Zou, *Catal. Today*, 2013, **212**, 81-88.
142 K. L. Erickson, T. E. Bostrom and R. L. Frost, *Mater. Lett.*, 2005, **59**, 226-229.
143 G. Carja, A. Nakajima, S. Dranca, C. Dranca and K. Okada, *J. Phys. Chem. C*, 2010, **114**, 14722-14728.
144 J. L. Gunjakar, T. W. Kim, H. N. Kim, I. Y. Kim and S. J. Hwang, *J. Am. Chem. Soc.*, 2011, **133**, 14998-15007.
145 M. Hadnadjev-Kostic, T. Vulic, J. Ranogajec, R. Marinkovic-Neducin and A. Radosavljevic-Mihajlovic, *J. Therm. Anal. Calorim.*, 2013, **111**, 1155-1162.
146 G. Carja, L. Dartu, K. Okada and E. Fortunato, *Chem. Eng. J.*, 2013, **222**, 60-66.
147 Y. F. Zhao, M. Wei, J. Lu, Z. L. Wang and X. Duan, *ACS Nano*, 2009, **3**, 4009-4016.
148 K. Dutta, S. Das and A. Pramanik, *J. Colloid Interface Sci.*, 2012, **366**, 28-36.
149 H. Fan, J. Y. Zhu, J. C. Sun, S. X. Zhang and S. Y. Ai, *Chem. Eur. J.*, 2013, **19**, 2523-2530.
150 E. M. Seftel, M. Mertens and P. Cool, *Appl. Catal. B: Environ.*, 2013, **134**, 274-285.
151 J. Y. Zhu, H. Fan, J. C. Sun and S. Y. Ai, *Sep. Purif. Technol.*, 2013, **120**, 134-140.
152 X. Liu, X. F. Zhao, Y. Zhu and F. Z. Zhang, *Appl. Catal. B: Environ.*, 2013, **140**, 241-248.
153 Z. J. Huang, P. X. Wu, Y. H. Lu, X. R. Wang, N. W. Zhu and Z. Dang, *J. Hazard. Mater.*, 2013, **246-247**, 70-78.
154 M. Nocchetti, A. Donnadio, V. Ambrogi, P. Andreani, M. Bastianini, D. Pietrella and L. Latterini, *J. Mater. Chem. B*, 2013, **1**, 2383-2393.
155 J. S. Valente, F. Tzompantzi, J. Prince, J. G. H. Cortez and R. Gomez, *Appl. Catal. B: Environ.*, 2009, **90**, 330-338.
156 L. Mohapatra and K. M. Parida, *Sep. Purif. Technol.*, 2012, **91**, 73-80.
157 D. Chen, Y. Li, J. Zhang, J. Z. Zhou, Y. Guo and H. Liu, *Chem. Eng. J.*, 2012, **185-186**, 120-126.
158 K. Parida, L. Mohapatra and N. Baliarsingh, *J. Phys. Chem. C*, 2012, **116**, 22417-22424.
159 J. G. Yu and X. X. Yu, *Environ. Sci. Technol.*, 2008, **42**, 4902-4907.
160 G. K. Zhang, M. Li, S. J. Yu, S. M. Zhang, B. B. Huang and J. G. Yu, *J. Colloid Interface Sci.*, 2010, **345**, 467-473.
161 S. J. Yu, G. K. Zhang, Y. Y. Gao and B. B. Huang, *J. Colloid Interface Sci.*, 2011, **354**, 322-330.
162 S. J. Xia, F. X. Liu, Z. M. Ni, J. L. Xue and P. P. Qian, *J. Colloid Interface Sci.*, 2013, **405**, 195-200.
163 X. Zong, H. J. Yan, G. P. Wu, G. J. Ma, F. Y. Wen, L. Wang and C. Li, *J. Am. Chem. Soc.*, 2008, **130**, 7176-7177.
164 A. Gasparotto, D. Barreca, D. Bekermann, A. Devi, R. A. Fischer, P. Fornasiero, V. Gombac, O. I. Lebedev, C. Maccato, T. Montini, G. Van Tendeloo and E. Tondello, *J. Am. Chem. Soc.*, 2011, **133**, 19362-19365.

165 X. Wang, Q. Xu, M. R. Li, S. Shen, X. L. Wang, Y. C. Wang, Z. C. Feng, J. Y. Shi, H. X. Han and C. Li, *Angew. Chem. Int. Ed.*, 2012, **51**, 13089-13092.

166 H. Tsuneoka, K. Teramura, T. Shishido and T. Tanaka, *J. Phys. Chem. C*, 2010, **114**, 8892-8898.

167 J. W. Liu, Y. Sun, Z. H. Li, S. Y. Li and J. X. Zhao, *Int. J. Hydrogen Energy*, 2011, **36**, 5811-5816.

168 S. X. Ouyang, H. Tong, N. Umezawa, J. Y. Cao, P. Li, Y. P. Bi, Y. J. Zhang and J. H. Ye, *J. Am. Chem. Soc.*, 2012, **134**, 1974-1977.

169 S. S. K. Ma, T. Hisatomi, K. Maeda, Y. Moriya and K. Domen, *J. Am. Chem. Soc.*, 2012, **134**, 19993-19996.

170 M. T. Li, J. Z. Su and L. J. Guo, *Int. J. Hydrogen Energy*, 2008, **33**, 2891-2896.

171 S. Shen, L. Zhao, Z. Zhou and L. Guo, *J. Phys. Chem. C*, 2008, **112**, 16148-16155.

172 J. Shen, J. T. Zai, Y. P. Yuan and X. F. Qian, *Int. J. Hydrogen Energy*, 2012, **37**, 16986-16993.

173 K. Kočí, L. Obalová, L. Matějová, D. Plachá, Z. Lacný, J. Jirkovský and O. Šolcová, *Appl. Catal. B: Environ.*, 2009, **89**, 494-502.

174 K. Kočí, K. Matějů, L. Obalová, S. Krejčíková, Z. Lacný, D. Plachá, L. Čapek, A. Hospodková and O. Šolcová, *Appl. Catal. B: Environ.*, 2010, **96**, 239-244.

175 Y. K. Kho, A. Iwase, W. Y. Teoh, L. Mädler, A. Kudo and R. Amal, *J. Phys. Chem. C*, 2010, **114**, 2821-2829.

176 N. M. Dimitrijevic, B. K. Vijayan, O. G. Poluektov, T. Rajh, K. A. Gray, H. He and P. Zapol, *J. Am. Chem. Soc.*, 2011, **133**, 3964-3971.

177 A. Gallo, T. Montini, M. Marelli, A. Minguzzi, V. Gombac, R. Psaro, P. Fornasiero and V. Dal Santo, *ChemSusChem*, 2012, **5**, 1800-1811.

178 Q. Liu, Y. Zhou, J. H. Kou, X. Y. Chen, Z. P. Tian, J. Gao, S. C. Yan and Z. G. Zou, *J. Am. Chem. Soc.*, 2010, **132**, 14385-14387.

179 X. Y. Chen, Y. Zhou, Q. Liu, Z. D. Li, J. G. Liu and Z. G. Zou, *ACS Appl. Mater. Interfaces*, 2012, **4**, 3372-3377.

180 P. Q. Wang, Y. Bai, P. Y. Luo and J. Y. Liu, *Catal. Commun.*, 2013, **38**, 82-85.

181 S. C. Yan, J. J. Wang, H. L. Gao, N. Y. Wang, H. Yu, Z. S. Li, Y. Zhou and Z. G. Zou, *Adv. Funct. Mater.*, 2013, **23**, 758-763.

182 Y. F. Zhao, P. Y. Chen, B. S. Zhang, D. S. Su, S. T. Zhang, L. Tian, J. Lu, Z. X. Li, X. Z. Cao, B. Y. i. Wang, M. Wei, D. G. Evans and X. Duan, *Chem. Eur. J.*, 2012, **18**, 11949-11958.

183 K. Parida, M. Satpathy and L. Mohapatra, *J. Mater. Chem.*, 2012, **22**, 7350-7357.

184 N. Baliarsingh, L. Mohapatra and K. Parida, *J. Mater. Chem. A*, 2013, **1**, 4236-4243.

185 N. Ahmed, Y. Shibata, T. Taniguchi and Y. Izumi, *J. Catal.*, 2011, **279**, 123-135.

186 N. Ahmed, M. Morikawa and Y. Izumi, *Catal. Today*, 2012, **185**, 263-269.

187 K. Teramura, S. Iguchi, Y. Mizuno, T. Shishido and T. Tanaka, *Angew. Chem. Int. Ed.*, 2012, **124**, 8132-8135.

Jin Liu received his MS degree at Wuhan University of Technology in 2012. He is currently a PhD candidate under the supervision of Professor Gaoke Zhang at School of Resources and Environmental Engineering, Wuhan University of Technology. His research interests include the design and synthesis of novel photocatalysts for water treatment.

Dr Gaoke Zhang is a full professor at School of Resources and Environmental Engineering, Wuhan University of Technology. From 2005 to 2006, he was an adjunct professor at Materials Research Institute, Pennsylvania State University. His research interests focus on clay-based materials, novel photocatalysts and adsorption materials for environmental applications.

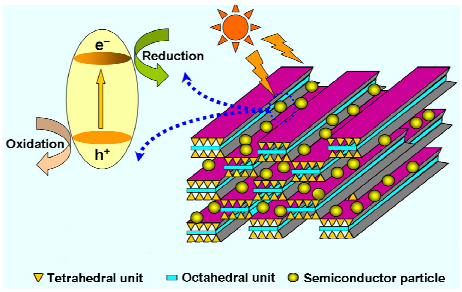

Highlight: Clay-based photocatalysts with high adsorbability and special structures have attracted extensive attention for their applications in environment and energy fields.